SOLAR CELLS

Metastable Dion-Jacobson 2D structure enables efficient and stable perovskite solar cells

Fei Zhang[1]*†, So Yeon Park[1]†, Canglang Yao[2,3]†, Haipeng Lu[1], Sean P. Dunfield[4,5,6], Chuanxiao Xiao[4], Soňa Uličná[7], Xiaoming Zhao[8], Linze Du Hill[9], Xihan Chen[1], Xiaoming Wang[2,3], Laura E. Mundt[7], Kevin H. Stone[7], Laura T. Schelhas[1,7], Glenn Teeter[4], Sean Parkin[10], Erin L. Ratcliff[9,11,12], Yueh-Lin Loo[8], Joseph J. Berry[4,5,13], Matthew C. Beard[1], Yanfa Yan[2,3]*, Bryon W. Larson[1]*, Kai Zhu[1]*

The performance of three-dimensional (3D) organic-inorganic halide perovskite solar cells (PSCs) can be enhanced through surface treatment with 2D layered perovskites that have efficient charge transport. We maximized hole transport across the layers of a metastable Dion-Jacobson (DJ) 2D perovskite that tuned the orientational arrangements of asymmetric bulky organic molecules. The reduced energy barrier for hole transport increased out-of-plane transport rates by a factor of 4 to 5, and the power conversion efficiency (PCE) for the 2D PSC was 4.9%. With the metastable DJ 2D surface layer, the PCE of three common 3D PSCs was enhanced by approximately 12 to 16% and could reach approximately 24.7%. For a triple-cation–mixed-halide PSC, 90% of the initial PCE was retained after 1000 hours of 1-sun operation at ~40°C in nitrogen.

P erovskite solar cells (PSCs) are a promising photovoltaic (PV) technology, and certified power conversion efficiencies (PCEs) as high as 25.5% have been reported (1). Despite this high performance, device stability hinders their commercialization. Efforts to improve device stability include defect passivation, contact layer modification, and encapsulation (2–5). The use of two-dimensional (2D) perovskite as the interfacial modification layer has great potential for addressing surface defects, in particular to improve the stability and efficiency of PSCs (6–8). The Ruddlesden-Popper (RP) 2D layered perovskites that are based on bulky cations, such as phenethylammonium (PEA$^+$) or butylammonium (BA$^+$), have been widely applied to the surface of 3D perovskite thin films to decrease defect densities and enhance device stability (8–11). Such bulky organic cations often self-assemble into a barrier layer

that protects against surface water adsorption or ingress. However, bulky-cation–based 2D structures often exhibit anisotropic and poor charge transport across the organic layer and are susceptible to charge-extraction barrier formation that inhibits efficient device operation (12–14).

We show a rational design strategy to maximize the out-of-plane hole transport based on a metastable Dion-Jacobson (DJ) 2D perovskite surface layer with a reduced transport energy barrier by using asymmetric bulky organic molecules, leading to highly efficient and stable perovskite solar cells. Our general design strategy to maximize the out-of-plane charge transport in 2D perovskites is illustrated in Fig. 1. Because the free electrons and holes are localized in the conduction band minimum (CBM) and valence band maximum (VBM) of the [PbI$_6$] planes, respectively, and because of

the long distance between two adjacent [PbI$_6$] planes, the out-of-plane charge transport must traverse the bulky cationic organic layers. Thus, it is mainly limited by two factors: (i) the low carrier mobility within the organic layer and (ii) the energy barrier between the [PbI$_6$] planes and the bulky organic cations. To mitigate the first limit, DJ 2D structures based on a short and single layer of divalent organoammonium cations (15–18) are generally more preferable than the RP 2D structures based on double layers of monovalent organoammonium cations (19). To mitigate the second limiting factor, the band offsets between the [PbI$_6$] planes and the bulky cationic organic layers need to be optimized.

The coupling (interaction) between [PbI$_6$] planes and the organic cations is through hydrogen bonding, and the change in the bonding strength can affect the band offsets (20). For a weaker hydrogen bonding configuration, the bonding states of the bulky organic layers are normally at a higher energy position, which brings them nearer the VBM of the [PbI$_6$] planes (Fig. 1A). This effect leads to a smaller band offset or barrier for hole transport between the [PbI$_6$] inorganic planes and organic cations. Because of the spin-orbital coupling of Pb 6p orbitals, the antibonding states of the organic layers are much higher than the CBM of the [PbI$_6$] planes. Thus, a DJ structure with weaker hydrogen bonding should improve hole transport. Yet, a weaker hydrogen bonding (or H-bonding) configuration generally means a less stable structure. Thus, a metastable DJ 2D structure with short cationic organic layers could in principle facilitate out-of-plane hole transport.

A rational strategy to induce the desired metastable H-bonding motifs in DJ 2D structures is to use asymmetric diammonium cations in lieu of symmetric straight chain divalent

Table 1. PV parameters of PSCs based on control and DMePDAI$_2$-modified perovskite thin films by using different perovskite compositions. V_{oc}, open-circuit voltage; FF, fill factor.

Device	Scan	J_{sc} (mA/cm^2)	V_{oc} (V)	FF	PCE (%)	SPO (%)
FA$_{0.85}$MA$_{0.1}$Cs$_{0.05}$PbI$_{2.9}$Br$_{0.1}$	Forward	24.35	1.111	0.773	20.9	20.4
	Reverse	24.32	1.099	0.764	20.4	
FA$_{0.85}$MA$_{0.1}$Cs$_{0.05}$PbI$_{2.9}$Br$_{0.1}$ /DMePDAI$_2$	Forward	24.97	1.167	0.822	24.0	23.7
	Reverse	24.93	1.167	0.814	23.7	
FA$_{0.97}$MA$_{0.03}$PbI$_{2.91}$Br$_{0.09}$	Forward	25.21	1.103	0.791	22.0	21.7
	Reverse	25.15	1.108	0.781	21.8	
FA$_{0.97}$MA$_{0.03}$PbI$_{2.91}$Br$_{0.09}$ /DMePDAI$_2$	Forward	25.25	1.158	0.843	24.7	24.3
	Reverse	25.26	1.158	0.839	24.5	
MAPbI$_3$	Forward	23.09	1.090	0.742	18.7	18.2
	Reverse	23.09	1.080	0.729	18.2	
MAPbI$_3$/DMePDAI$_2$	Forward	23.19	1.131	0.797	20.9	20.8
	Reverse	23.19	1.132	0.794	20.8	

cations. For example, both *N,N*-dimethyl-1,3-propane diammonium (DMePDA^{2+}) and 1,4-butane diammonium (BDA^{2+}) form DJ 2D structures with short interlayer distances [19]. Whereas BDA^{2+} is symmetric and features two terminal primary ammonium ions on the butyl (C4) chain, DMePDA^{2+} is asymmetric, with a primary ammonium on one end and a dimethyl-substituted tertiary ammonium on the other end of the propyl (C3) chain. The "head or tail" H-bonding options for the DMePDA^{2+} molecules are asymmetric, giving rise to different possible relative orientations of the adjacent molecules, and the different H-bonding interactions possible within the [PbI$_6$] planes could lead to both stable and metastable energy polymorphs of the 2D structure (Fig. 1B). The alternating relative head-to-tail alignment of adjacent DMePDA^{2+} cations (most stable orientation configuration) provides a larger compensation for overall structural relaxation than those of other orientation arrangements. By contrast, the

symmetric BDA^{2+} molecule has only one possible orientation configuration (Fig. 1B) and cannot form metastable polymorphs.

We further examined single-crystal 2D DJ structures from BDAI$_2$ and DMePDAI$_2$ and conducted first-principle calculations to verify our design strategy. We found that 1,3-propane diammonium diiodine (PDAI$_2$)—which is often assumed the shortest diamine [15, 21] to form DJ 2D perovskites—templated Pb-I to a non-perovskite structure (empirical formula: [PDAPbI$_4$]$_{15}$•[PDAI$_2$]) (fig. S1 and table S1). Thus, BDA^{2+} represents the shortest linear-alkyl-chain diamine that forms an iodide-based 2D DJ structure (BDAPbI$_4$) (fig. S2A and table S2). C3-based DMePDAI$_2$ with two methyl groups attached to one side of PDA can form 2D DJ structures with two polymorphs, which we refer to as DMePDAPbI$_4$-1 (fig. S2B and table S3) and DMePDAPbI$_4$-2, respectively (fig. S2C) [22].

We grew the DMePDAPbI$_4$-1 single crystal, which was based on the most stable DMePDA^{2+} orientation alignment, from a

concentrated hydroiodic acid solution using a slow-crystallization process, as adapted from our previous report [23] and consistent with a previous theoretical predication [24]. By contrast, the DMePDAPbI$_4$-2 single crystal, which was based on a metastable orientational alignment, was formed from either a fast cooling [22] or antisolvent quenching during single-crystal growth [25], both of which represent a fast-crystallization process. In comparison with DMePDAPbI$_4$-1, DMePDAPbI$_4$-2 had an emission wavelength that was red-shifted ~25 nm, which is consistent with the corresponding absorption data (fig. S3). The average interlayer distances were comparable among these 2D structures (~10.10 to 10.39 Å), with that of BDAPbI$_4$ being the shortest. The corresponding hydrogen-bonding configurations for these three single-crystal structures (figs. S4, S5, and S6) were consistent with the analysis in Fig. 1B.

We confirmed our design strategy by means of density functional theory (DFT) calculation.
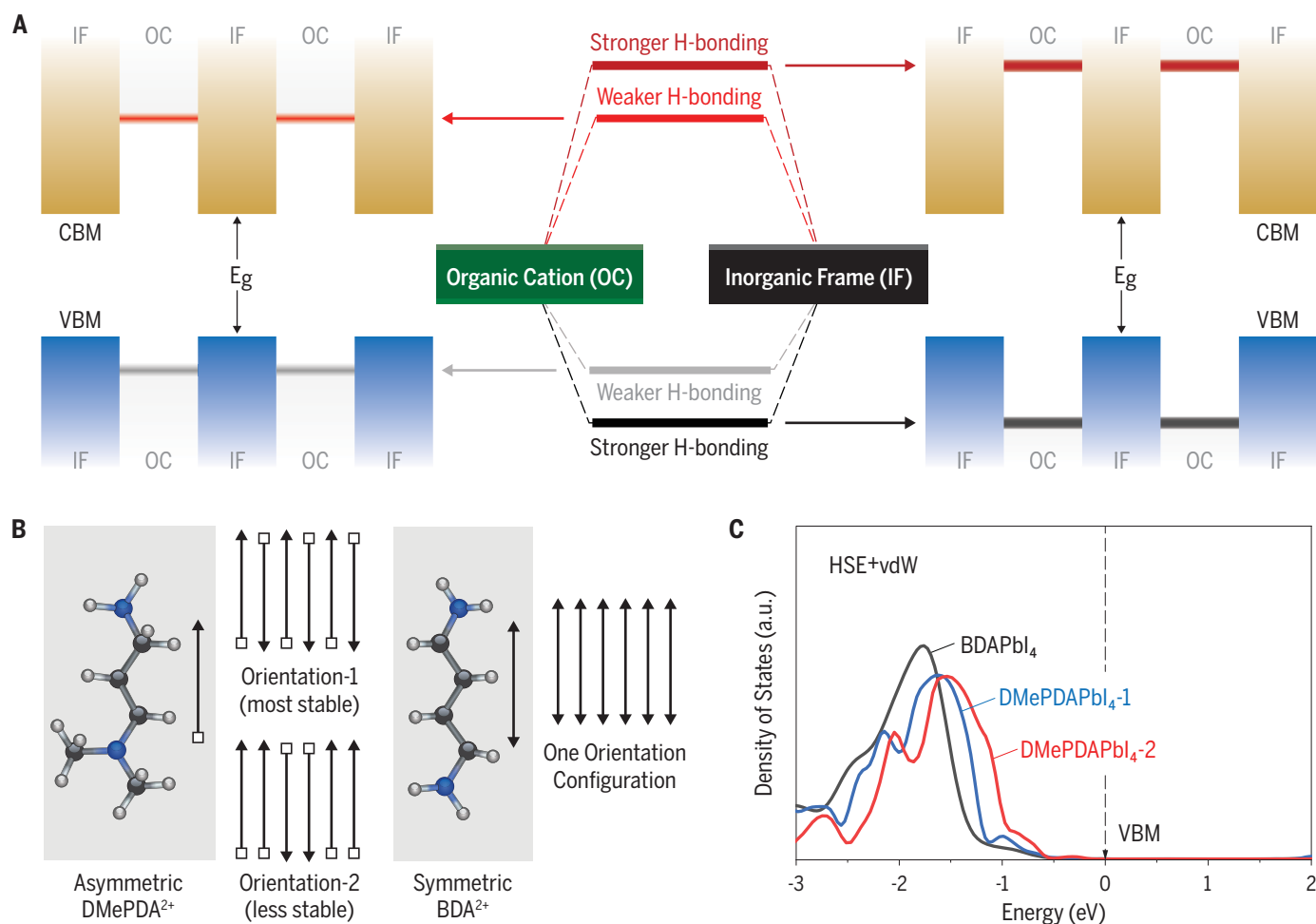
Fig. 1. Design concept. (**A**) Illustration of band offsets between [PbI$_6$] planes and bulky organic cations with a weaker and stronger degree of H-bonding. For clarity, the inorganic framework orbital diagram is omitted in the middle of the panel. (**B**) Two possible arrangements of asymmetric DMePDA^{2+} cations and the sole arrangement of symmetric BDA^{2+} cations. (**C**) HSE+vdW calculated total DOSs of the organic cations in BDAPbI$_4$, DMePDAPbI$_4$-1 [with orientation-1 in (B)], and DMePDAPbI$_4$-2 [with orientation-2 in (B)]. The VBMs were set to 0.0 eV.

We calculated the effect of organic molecules using the screened hybrid functional and van der Waals (vdW) interaction (HSE+vdW) (26, 27). The DMePDAPbI$_4$-2 structure was indeed less stable than the DMePDAPbI$_4$-1 structure. The energy level differences of the organic cations in BDAPbI$_4$, DMePDAPbI$_4$-1, and DMePDAPbI$_4$-2 could be seen in the total density of states (DOSs) of the organic cations (the sum of states of C, N, and H atoms) (Fig. 1C). The total DOS of BDA^{2+} cations in BDAPbI$_4$ was lower in energy (farther from VBM) than that of DMePDA^{2+} cations in DMePDAPbI$_4$-1, which in turn was lower in energy compared with the total DOS of DMePDA^{2+} cations in DMePDAPbI$_4$-2. Thus, we expected the out-of-plane hole transport to improve from BDAPbI$_4$ to DMePDAPbI$_4$-2.

Rapid perovskite film growth conditions from standard solution deposition also led to the formation of the metastable DMeP-DAPbI$_4$-2 structure. The XRD patterns of the DMePDAPbI$_4$ thin film prepared by means of spin coating are shown in Fig. 2A. The powder XRD pattern measured from DMePDAPbI$_4$-1 and DMePDAPbI$_4$-2 single-crystal samples, along with the calculated powder XRD patterns shown in Fig. 2A for comparison, revealed the differences of XRD patterns between these two single crystals. The XRD pattern of

the thin-film sample matched that of the DMePDAPbI$_4$-2 structure. A metastable polymorph does not mean it is unstable under synthetic or ambient conditions. The phase transformation between polymorphs requires 180° rotation of the alkyl chain, which is highly energetically unfavorable (Fig. 2B) (figs. S7 and S8). A wide range of thin-film growth conditions from solution all formed DMePDAPbI$_4$-2 thin films (fig. S9).

To test our hypothesis that the reduced energy barrier from the asymmetric bulky organic cation layer could facilitate charge transport between inorganic [PbI$_6$] sheets, we conducted time-resolved microwave conductivity (TRMC) measurements along the out-of-plane direction (28). In Fig. 2C, we compare the normalized TRMC results between several n = 1 2D perovskite thin films calibrated by their corresponding internal quantum yield of charges measured in devices. The out-of-plane transport for DMePDAPbI$_4$ (or more specifically, DMePDAPbI$_4$-2) is about a factor of 4 to 5 faster than that of BDAPbI$_4$, despite the slightly longer interlayer distance. Space-charge–limited current (SCLC) measurements further verified that the DMeP-DAPbI$_4$-2 structure had faster out-of-plane hole transport than that of the DMePDAPbI$_4$-1 structure (fig. S10). These results confirmed

the role of reducing the energy barrier for improving out-of-plane charge transport. The out-of-plane transport for the two 2D DJ structures (DMePDAPbI$_4$ and BDAPbI$_4$) was faster than those of the two 2D RP structures (BA$_2$PbI$_4$ and PEA$_2$PbI$_4$). These TRMC results were consistent with the current density-voltage (J–V) results of PSCs on the basis of the corresponding n = 1 2D structures (Fig. 2D and table S4). The DMePDAPbI$_4$-based PSC reached a PCE of 4.90% (forward scan) and 4.33% (reverse scan), which is among the highest obtained thus far for any n = 1 2D lead iodide–based PSCs (6); the corresponding external quantum efficiency (EQE) spectrum is shown in fig. S11.

The use of 2D systems to passivate defects and enhance performance has recently been used in many polycrystalline PV technologies (29). We validated the impact of this metastable design motif with the use of DMePDAPbI$_4$ as a surface layer to improve the quality of 3D perovskite absorbers. We spin-coated the corresponding bulky organic halide salt in isopropanol (IPA) solution on top of a 3D perovskite absorber layer (6). Specifically, the DMePDAI$_2$/IPA solution was coated atop (FAPbI$_3$)$_{0.85}$(MAPbI$_2$Br)$_{0.1}$(CsPbI$_3$)$_{0.05}$ (or FA$_{0.85}$MA$_{0.1}$Cs$_{0.05}$PbI$_{2.9}$Br$_{0.1}$) followed by annealing, where FA is formamidinium and MA is methylammonium. The thin-film XRD

Fig. 2. 2D thin-film structure, transport, and device characteristics. (A) XRD patterns of a solution-grown DMePDAPbI$_4$ thin film and the powder XRD patterns (measured and calculated) from DMePDAPbI$_4$-1 and DMePDAPbI$_4$-2 single-crystal structures. X-ray source, Cu Kα radiation. The peak labeled with an asterisk is from the fluorine tin oxide (FTO) substrates. **(B)** Energy profile along the transition path between DMePDAPbI$_4$-1 and DMePDAPbI$_4$-2. **(C)** TRMC comparison of out-of-plane charge transport across the layers of n = 1 2D perovskites. **(D)** J–V characteristics of PSCs based on n = 1 2D perovskite thin films using a device stack of glass/FTO/compact-TiO$_2$/2D-perovskite/2,2',7,7'-Tetrakis[N,N-di(4-methoxyphenyl)amino]-9,9'-spirobifluorene (spiro-OMeTAD)/Au.
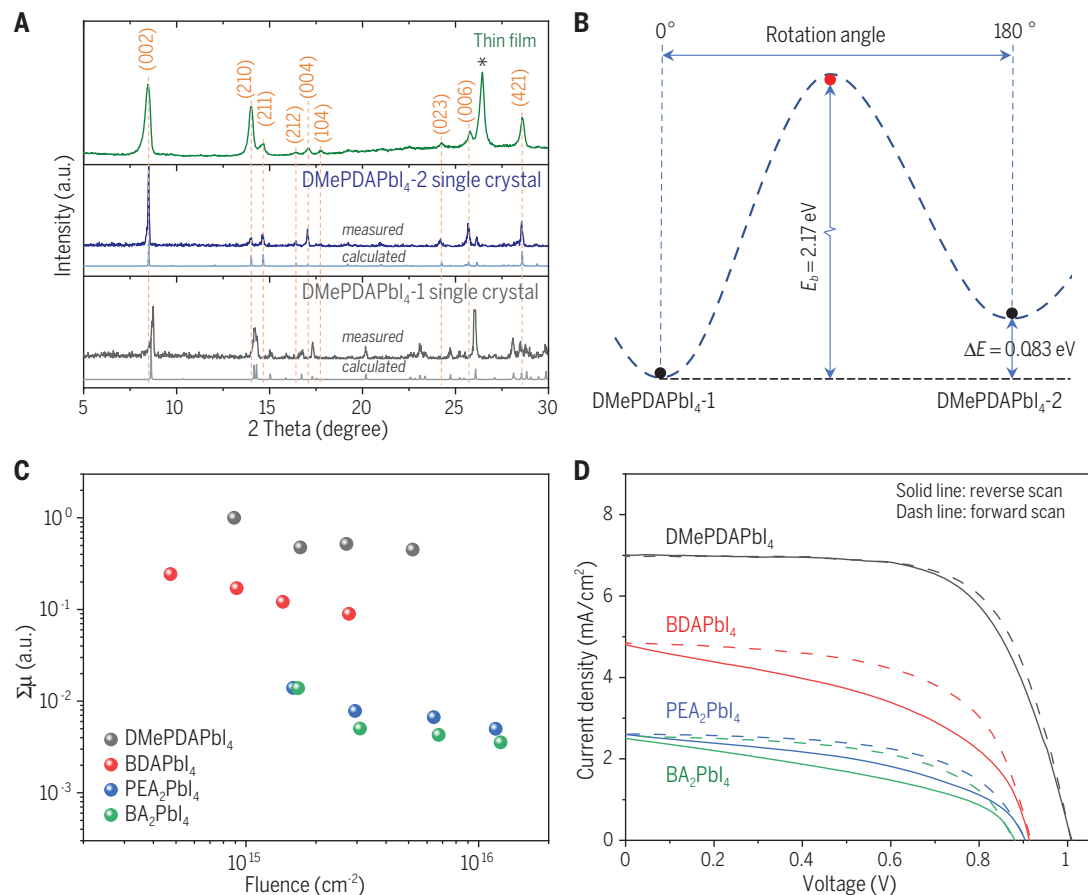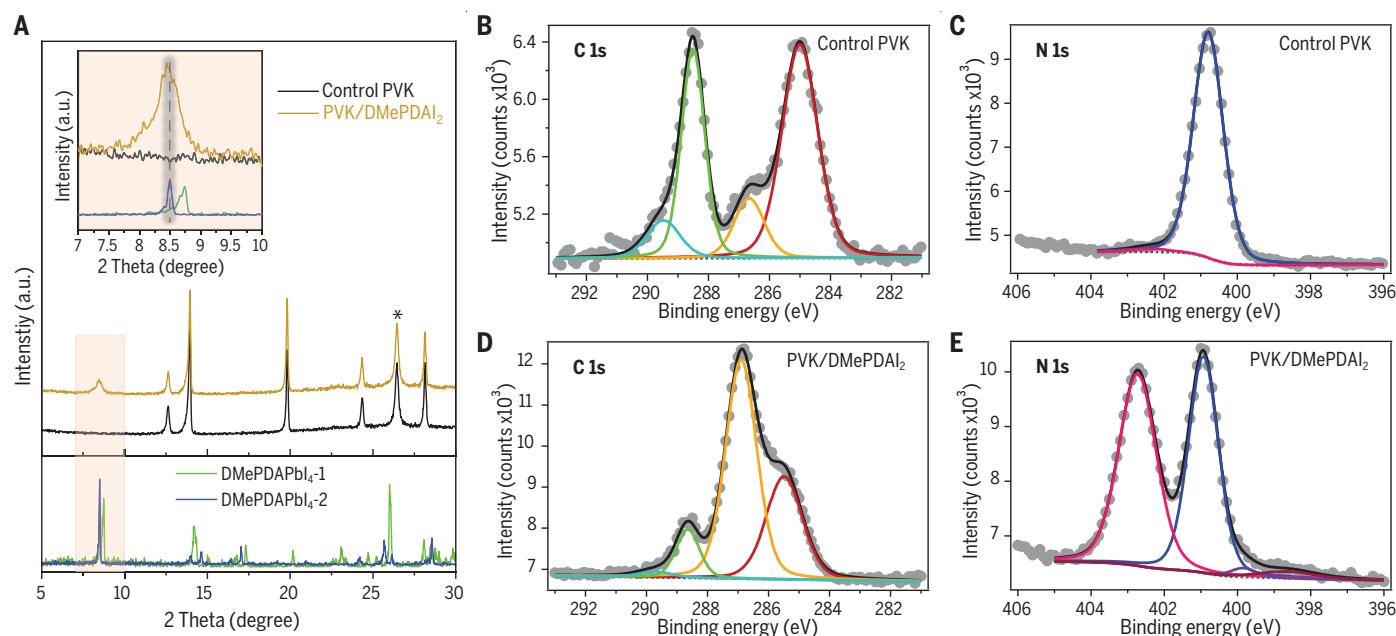
Fig. 3. Surface layer treatment. (**A**) Comparison of grazing incident XRD (GIXRD) patterns of thin films of DMePDAPbI$_4$ and perovskites without (control PVK) and with DMePDAI$_2$ surface treatment (PVK/DMePDAI$_2$). (Inset) Zoom-in view of the GIXRD pattern from 7° to 10°. The peak labeled with an asterisk is from the FTO substrate. X-ray source, Cu Kα radiation. (**B** to **E**) Comparison of the XPS spectra of N1s and C1s for [(B) and (C)] the control and [(D) and (E)] the DMePDAI$_2$-modified perovskite thin film.

results suggested that the DMePDAPbI$_4$-2 structure formed, as evidenced by the characteristic low-angle diffraction peak, at ~8.5° for DMePDAPbI$_4$-2, rather than ~8.7° for DMePDAPbI$_4$-1 (Fig. 3A).

We also checked the 2D structures on top of three other common perovskite compositions of Cs$_{0.05}$FA$_{0.95}$PbI$_3$, (FAPbI$_3$)$_{0.95}$(MAPbBr$_3$)$_{0.05}$, and FAPbI$_3$ (fig. S12). For these compositions, the characteristics peaks at (002), (004), and (006) matched well to DMePDAPbI$_4$-2, which were absent in the DMePDAPbI$_4$-1 spectrum. Last, the low-angle diffraction peak associated with the 2D structure from the thin-film XRD results were further confirmed with grazing-incidence wide-angle x-ray scattering (GIWAXS) measurements (fig. S13). In terms of 2D surface-layer topology and coverage, the scanning electron microscopy (SEM) measurements indicated that the treatment induced formation of a thin surface layer with small apparent grain sizes (figs. S14 and S15). The conductive-atomic force microscopy (C-AFM) measurements show that the current of the treated film is much more uniform and lower than that of the control film, which is consistent with the formation of a capping layer over the 3D perovskite layer (fig. S16).

To gain more insight into how the DMeP-DAI$_2$ modification affects the optoelectronic properties in perovskite films, we conducted steady-state photoluminescence (PL), time-resolved photoluminescence (TRPL), and TRMC studies on these samples. The DMePDAI$_2$ treatment led to enhanced PL intensity (fig.

S17), longer TRPL lifetime (fig. S18 and table S5), and improved TRMC mobility and lifetime (fig. S19) that were consistent with the improved surface properties (*8, 30*). In addition, the ultraviolet photoelectron spectroscopy (UPS) measurements showed that the 2D surface treatment improved the energetics for hole transport from the 3D perovskite to the 2D surface layer (fig. S20).

The impact of the DMePDAI$_2$ treatment on the perovskite surface chemistry was investigated with x-ray photoelectron spectroscopy (XPS). Normalized core levels from key elements identified on the sample surface are included in figs. S21 and S22. The spectral shapes of most core levels showed minimal change between the two samples, indicating similar bonding environments, but surface treatment caused change in the C 1s and N 1s core levels. We fit the core levels (Fig. 3, B to E) using constrained fitting procedures (summarized in tables S6 and S7). The control sample had a N 1s region whose relative peak areas were dominated by a C=NH$_2^+$ (FA) peak (~401 eV) with a small shoulder to higher binding energy (~403 eV) that corresponded to C–NH$_3$ (MA). The DMePDAI$_2$ treatment increased the area of the C–NH$_3$ peak and also led to two additional peaks at a lower binding energy consistent with that of C–NH$_2$ (~400 eV) and the tertiary amine in DMePDAI$_2$ (~398 eV). Concomitant with these changes, redistribution occurred in the features in the C 1s spectra comprising four main peaks that are consistent with primarily C–C or C–H (~285 eV),

N–CH$_3$ (~287 eV), HC(NH$_2$)$_2$ (~289 eV), and C–O or C=O bonds (~290 eV). The surface treatment decreased the concentration of HC(NH$_2$)$_2$ bonds from FA on the surface while simultaneously increasing the amount of N–CH$_3$ and C–C or C–H bonds. In addition, XPS revealed that surface treatment increased the amount of halide on the surface, from about 2.6 halide-to-lead ratio for the control to 3.1 for the DMePDAI$_2$-treated film. Collectively, these results suggest that both organic and halide components of the additive incorporated into the top surface of the treated films. Undercoordinated lead can cause donor defects on the surface, resulting in downward band bending and increased recombination centers (*31*), so the increase in the halide-to-lead ratio associated with the formation of 2D interfacial component upon surface treatment was consistent with a less defective surface.

We investigated the impact of DMePDAI$_2$ surface treatment on the PV performance by fabricating PSCs using the standard n-i-p device architecture, glass/FTO/electron transport layer (ETL)/perovskite/hole transport layer (HTL)/ Au, where ETL is TiO$_2$ or SnO$_2$ and HTL is spiro-OMeTAD, with more details in the supplementary materials (*23*). Typical cross-section SEM images of devices are shown in fig. S23. In Fig. 4A, we compare the *J–V* curves of the PSCs on the basis of triple-cation–mixed-halide FA$_{0.85}$MA$_{0.1}$Cs$_{0.05}$PbI$_{2.9}$Br$_{0.1}$ without and with DMePDAI$_2$ treatment under simulated 100-mW/cm^2 air mass coefficient (AM) 1.5 G
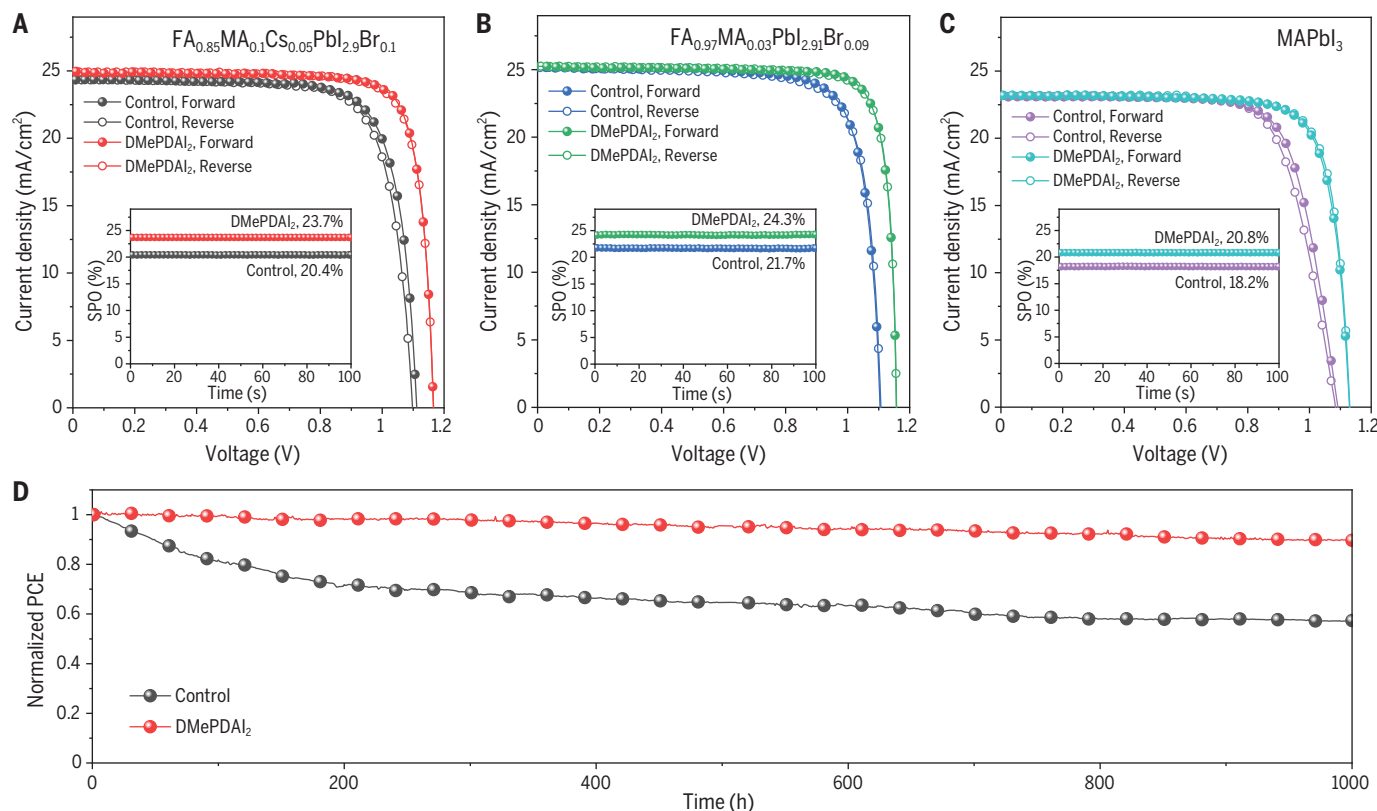
Fig. 4. Device characteristics. (**A** to **C**) *J–V* characteristics of PSCs based on different perovskite compositions. (A) $FA_{0.85}MA_{0.1}Cs_{0.05}PbI_{2.9}Br_{0.1}$. (B) $FA_{0.97}MA_{0.03}PbI_{2.91}Br_{0.09}$. (C) $MAPbI_3$. (Insets) SPOs of the corresponding devices. (**D**) Operation ISOS-L-1 stability (maximum power point tracking, in N_2, continuous one-sun illumination at ~40°C) of unencapsulated PSC based on $FA_{0.85}MA_{0.1}Cs_{0.05}PbI_{2.9}Br_{0.1}$. The initial PCE was 20.5% for the control and 23.1% for the $DMePDAI_2$-treated device.

illumination (Table 1). With the surface treatment, the device PCE increased from about 20.9 to 24.0% from forward scan and from 20.4 to 23.7% from reverse scan. The PCE improvement is also consistent with a better perovskite-HTL junction on the basis of the cross-sectional Kelvin probe force microscopy (KPFM) measurements (fig. S24) (*32*). The optimum concentration for $DMePDAI_2$-surface treatment was found at 0.5 mg/mL (fig. S25).

In addition to the $FA_{0.85}MA_{0.1}Cs_{0.05}PbI_{2.9}Br_{0.1}$ perovskite composition, we also examined the impact of $DMePDAI_2$ surface treatment on PSCs on the basis of double-cation–mixed-halide ($FA_{0.97}MA_{0.03}PbI_{2.91}Br_{0.09}$) and single-cation–single-halide ($MAPbI_3$) using ETL of SnO_2 and TiO_2, respectively, and found PCE improvements for both compositions (Fig. 4, B and C). Noteworthy for PSCs based on $FA_{0.97}MA_{0.03}PbI_{2.91}Br_{0.09}$, the PCE was improved from 22.0 to 24.7% from forward scan and from 21.8 to 24.5% from reverse scan, with short-circuit current density (J_{sc}) > 25 mA/cm², which is in agreement with the EQE spectrum (fig. S26). For all three perovskite compositions, the stabilized power outputs (SPOs) for PSCs based on the control and $DMePDAI_2$-modified perovskite thin films matched well with the *J–V* measurements (Fig. 4, A to C, insets, and Table 1). The PCE improvement for all three perovskite compositions was reproducible on the basis of the statistical comparison (fig. S27). The devices with this treatment also exhibited higher PCE than that of devices based on other surface treatments with similar length of bulky organic salts for either RP or DJ 2D perovskites (fig. S28).

Last, we checked the operation stability of unencapsulated $FA_{0.85}MA_{0.1}Cs_{0.05}PbI_{2.9}Br_{0.1}$–based PSCs using maximum power point (MPP) tracking at ~40°C in N_2, following the ISOS-L-1 stability protocol (*33*). The $DMePDAI_2$-modified PSC (Fig. 4D) showed only 10% relative efficiency drop after 1000 hours of continuous operation, whereas the PCE of the control device decreased by ~43%. The stability improvement with $DMePDAI_2$ surface treatment was also observed when the devices were tested at high-moisture (>85% relative humidity) or high-temperature (85°C) conditions (figs. S29 and S30). These results suggest that the $DMePDAI_2$-modification to form a 2D DJ phase surface layer is a general way to improve PSC performance. Our use of the metastable 2D DJ structure through hydrogen bonding tuning based on asymmetric bulky organic molecules represents a promising chemical design element for perovskite interfacial engineering to enhance PSC efficiency and stability.

REFERENCES AND NOTES

1. National Renewable Energy Laboratory, Best research-cell efficiency chart (August, 2020); www.nrel.gov/pv/cell-efficiency.html.
2. D. Bi *et al.*, *Nat. Energy* **1**, 16142 (2016).
3. X. Zheng *et al.*, *Nat. Energy* **2**, 17102 (2017).
4. F. Zhang *et al.*, *Adv. Mater.* **29**, 1606806 (2017).
5. X. Li *et al.*, *Nat. Chem.* **7**, 703–711 (2015).
6. F. Zhang *et al.*, *Energy Environ. Sci.* **13**, 1154–1186 (2020).
7. E. H. Jung *et al.*, *Nature* **567**, 511–515 (2019).
8. H. Min *et al.*, *Science* **366**, 749–753 (2019).
9. L. Liang, H. Luo, J. Hu, H. Li, P. Gao, *Adv. Energy Mater.* **10**, 2000197 (2020).
10. Y.-W. Jang *et al.*, *Nat. Energy* **6**, 63–71 (2021).
11. J. Xue *et al.*, *Science* **371**, 636–640 (2021).
12. D. Thrithamarassery Gangadharan, D. Ma, *Energy Environ. Sci.* **12**, 2860–2889 (2019).
13. E. Shi *et al.*, *Nature* **580**, 614–620 (2020).
14. Y. Gao *et al.*, *Nat. Chem.* **11**, 1151–1157 (2019).
15. S. Ahmad *et al.*, *Joule* **3**, 794–806 (2019).
16. L. Mao *et al.*, *J. Am. Chem. Soc.* **140**, 3775–3783 (2018).
17. Y. Lv *et al.*, *J. Mater. Chem. A Mater. Energy Sustain.* **8**, 10283–10290 (2020).
18. X. Jiang *et al.*, *Nano Energy* **75**, 104892 (2020).
19. X. Li, J. M. Hoffman, M. G. Kanatzidis, *Chem. Rev.* **121**, 2230–2291 (2021).
20. G. Miessler, P. Fischer, D. Tarr, *Inorganic Chemistry* (Prentice Hall, ed. 5, 2014).
21. C. Ma, D. Shen, T.-W. Ng, M.-F. Lo, C.-S. Lee, *Adv. Mater.* **30**, 1800710 (2018).

22. T. Yu, L. Zhang, J. Shen, Y. Fu, Y. Fu, *Dalton Trans.* **43**, 13115–13121 (2014).
23. F. Zhang *et al.*, *Chem* **7**, 774–785 (2021).
24. S. Silver, S. Xun, H. Li, J.-L. Brédas, A. Kahn, *Adv. Energy Mater.* **10**, 1903900 (2020).
25. W. Zhao *et al.*, *J. Mater. Chem. A Mater. Energy Sustain.* **8**, 9919–9926 (2020).
26. A. V. Krukau, O. A. Vydrov, A. F. Izmaylov, G. E. Scuseria, *J. Chem. Phys.* **125**, 224106 (2006).
27. S. Grimme, J. Antony, S. Ehrlich, H. Krieg, *J. Chem. Phys.* **132**, 154104 (2010).
28. F. Zhang *et al.*, *J. Am. Chem. Soc.* **141**, 5972–5979 (2019).
29. D. L. McGott *et al.*, *Joule* **5**, 1057–1073 (2021).
30. H. Zhu *et al.*, *J. Am. Chem. Soc.* **143**, 3231–3237 (2021).
31. S. P. Dunfield *et al.*, *Adv. Energy Mater.* **10**, 1904054 (2020).
32. Y. Hou *et al.*, *Science* **367**, 1135–1140 (2020).
33. M. V. Khenkin *et al.*, *Nat. Energy* **5**, 35–49 (2020).

SUPPLEMENTARY MATERIALS

Science

Metastable Dion-Jacobson 2D structure enables efficient and stable perovskite solar cells

Fei ZhangSo Yeon ParkCanglang YaoHaipeng LuSean P. DunfieldChuanxiao XiaoSo#a Uli#náXiaoming ZhaoLinze Du HillXihan ChenXiaoming WangLaura E. MundtKevin H. StoneLaura T. SchelhasGlenn TeeterSean ParkinErin L. RatcliffYueh-Lin LooJoseph J. BerryMatthew C. BeardYanfa YanBryon W. LarsonKai Zhu

Directing efficient hole transport

Surface defects in three-dimensional perovskites can decrease performance but can be healed with coatings based on two-dimensional (2D) perovskite such as Ruddlesden-Popper phases. However, the bulky organic groups of these 2D phases can lead to low and anisotropic charge transport. F. Zhang *et al.* show that a metastable polymorph of a Dion-Jacobson 2D structure based on asymmetric organic molecules reduced the energy barrier for hole transport and their transport through the layer. When used as a top layer for a triple-cation mixed-halide perovskite, a solar cell retained 90% of its initial power conversion efficiency of 24.7% after 1000 hours of operation at approximately 40°C in nitrogen. —PDS

View the article online
https://www.science.org/doi/10.1126/science.abj2637
Permissions
https://www.science.org/help/reprints-and-permissions

Use of this article is subject to the Terms of service